AMERICAN SOCIETY FOR MICROBIOLOGY | mBio®

RESEARCH ARTICLE

Structural Elucidation of a Protective B Cell Epitope on Outer Surface Protein C (OspC) of the Lyme Disease Spirochete, *Borreliella burgdorferi*

Michael J. Rudolph,[a] Simon A. Davis,[a] H. M. Emranul Haque,[b] David D. Weis,[b] David J. Vance,[c] Carol Lyn Piazza,[c] Monir Ejemel,[d] Lisa Cavacini,[d] Yang Wang,[d] M. Lamine Mbow,[e]* Robert D. Gilmore,[e] Nicholas J. Mantis[c]

[a]New York Structural Biology Center, New York, New York, USA
[b]Department of Chemistry, University of Kansas, Lawrence, Kansas, USA
[c]Division of Infectious Diseases, Wadsworth Center, New York State Department of Health, Albany, New York, USA
[d]MassBiologics of the University of Massachusetts Chan Medical School, Boston, Massachusetts, USA
[e]Division of Vector Borne Diseases, National Center for Emerging and Zoonotic Infectious Diseases, Centers for Disease Control and Prevention, Fort Collins, Colorado, USA

ABSTRACT Outer surface protein C (OspC) plays a pivotal role in mediating tick-to-host transmission and infectivity of the Lyme disease spirochete, *Borreliella burgdorferi*. OspC is a helical-rich homodimer that interacts with tick salivary proteins, as well as components of the mammalian immune system. Several decades ago, it was shown that the OspC-specific monoclonal antibody, B5, was able to passively protect mice from experimental tick-transmitted infection by *B. burgdorferi* strain B31. However, B5's epitope has never been elucidated, despite widespread interest in OspC as a possible Lyme disease vaccine antigen. Here, we report the crystal structure of B5 antigen-binding fragments (Fabs) in complex with recombinant OspC type A ($OspC_A$). Each OspC monomer within the homodimer was bound by a single B5 Fab in a side-on orientation, with contact points along OspC's α-helix 1 and α-helix 6, as well as interactions with the loop between α-helices 5 and 6. In addition, B5's complementarity-determining region (CDR) H3 bridged the OspC-OspC′ homodimer interface, revealing the quaternary nature of the protective epitope. To provide insight into the molecular basis of B5 serotype specificity, we solved the crystal structures of recombinant OspC types B and K and compared them to $OspC_A$. This study represents the first structure of a protective B cell epitope on OspC and will aid in the rational design of OspC-based vaccines and therapeutics for Lyme disease.

IMPORTANCE The spirochete *Borreliella burgdorferi* is a causative agent of Lyme disease, the most common tickborne disease in the United States. The spirochete is transmitted to humans during the course of a tick taking a bloodmeal. After *B. burgdorferi* is deposited into the skin of a human host, it replicates locally and spreads systemically, often resulting in clinical manifestations involving the central nervous system, joints, and/or heart. Antibodies directed against *B. burgdorferi*'s outer surface protein C (OspC) are known to block tick-to-host transmission, as well as dissemination of the spirochete within a mammalian host. In this report, we reveal the first atomic structure of one such antibody in complex with OspC. Our results have implications for the design of a Lyme disease vaccine capable of interfering with multiple stages in *B. burgdorferi* infection.

KEYWORDS *Borreliella burgdorferi*, Lyme disease, X-ray crystallography, monoclonal antibodies, spirochetes, vaccines

Lyme disease (LD), or Lyme borreliosis (LB), is the most common tick-borne infection in North America and Europe. Clinical manifestations commonly associated with LD include erythema migrans, neuroborreliosis, carditis, and Lyme arthritis (1, 2). In North America, the primary etiological agent of LD is the spirochete *Borreliella burgdorferi*,

Editor Alan G. Barbour, University of California, Irvine

Address correspondence to Nicholas J. Mantis, Nicholas.Mantis@health.ny.gov, or Michael J. Rudolph, mrudolph@nysbc.org.

*Present address: M. Lamine Mbow, Boehringer Ingelheim Pharmaceuticals, Ridgefield, CT, USA.

The authors declare no conflict of interest.

Received 23 November 2022
Accepted 28 February 2023
Published 28 March 2023

while in Eurasia LD is caused by related genospecies, including *B. afzelii* and *B. garinii* (3, 4). In the United States, *B. burgdorferi* is vectored by blacklegged ticks, *Ixodes scapularis* and *Ixodes pacificus*. Naive tick larvae acquire *B. burgdorferi* during a blood meal on an infected reservoir species, including birds and an array of small mammals. Once within a tick, the spirochetal bacteria remain dormant in the midgut until a second blood meal taken during the nymphal stage, after which *B. burgdorferi* migrates to the salivary glands, where it is deposited into the skin of an impending host. Perpetuation of *B. burgdorferi*'s enzootic cycle and persistence within vertebrate reservoirs is contingent on the spirochete's ability to evade innate and adaptive immune responses through a myriad of mechanisms, including complement resistance, antigenic diversification, antigenic variation, and redundant adhesins and colonization factors (5–8).

With an estimated 476,000 individuals treated for Lyme disease per year in the United States (9), there is an acute need for vaccines that prevent *B. burgdorferi* transmission and limit human infections (10–12). An LD vaccine known as LYMErix was formerly approved for use in the United States but discontinued in 2002 for a variety of reasons (10, 12, 13). That vaccine, which consisted of recombinant outer surface protein A (OspA), elicited antibodies that blocked transmission of *B. burgdorferi* by interfering with egress of the spirochete from the tick midgut during the course of a blood meal (14–17). Second-generation OspA-based vaccines are currently in development and clinical trials (18, 19). One shortcoming of these vaccines is that once an infection is established, OspA antibodies are of little consequence, as surface expression of OspA is downregulated by *B. burgdorferi* within its mammalian host (20, 21).

Outer surface protein C (OspC; BBB19) has long been considered as another candidate LD vaccine antigen. OspC is an ~23-kDa helical-rich lipoprotein expressed by *B. burgdorferi* in the tick midgut during the course of a blood meal (22–27). OspC facilitates migration of *B. burgdorferi* from the midgut to the salivary glands and contributes to early stages of mammalian survival (22, 26, 28, 29). In the mouse model, OspC antibodies elicited through active or passive vaccination prevent tick-mediated *B. burgdorferi* infection (30, 31). Indeed, reminiscent of OspA, recent evidence indicates that OspC antibodies entrap *B. burgdorferi* within the tick midgut by a mechanism that does not involve direct spirochete killing (32). OspC antibodies also protect mice against *B. burgdorferi* needle infection and have been reported to promote resolution of arthritis and carditis in a SCID mouse model of Lyme disease (30, 33–37). Indeed, OspC-specific antibodies are associated with serum borreliacidal activity from early LD patients (38, 39). Thus, OspC antibodies afford a double layer of protection by interfering with *B. burgdorferi* tick-to-host transmission and promoting clearance of spirochetes that gain access to a mammalian host.

A potential drawback of OspC-based vaccines is that OspC is highly polymorphic within and across *B. burgdorferi* genospecies. At least 25 different *ospC* alleles or OspC types (when referring to the protein) have been identified to date, with extensive diversity occurring even within *B. burgdorferi* isolates within limited geographical regions (40–45). The degree of variability is such that antibody responses to a given OspC type have limited cross-reactivity with other OspC types (32, 33, 37, 46). Moreover, susceptibility to *B. burgdorferi* reinfection as well as repeated episodes of LD has been linked to OspC variability and immunodominance (30, 32, 33, 38, 41, 47–49). Thus, a vaccine based on a single OspC type would have limited utility in regions where multiple *B. burgdorferi* OspC types coexist.

To overcome this challenge, investigative teams have employed multiple sequence alignments, linear B cell epitope analysis, and computational modeling to localize conserved and type-specific residues on OspC associated with protection (41, 42, 50–55). This approach has proven fruitful, as Marconi and colleagues have developed multivalent chimeric vaccines for veterinary use that consist of conserved or minimally variable OspC epitopes from different OspC types (53, 56). In mice, chimeric OspC vaccines elicit broadly reactive antibodies with complement-dependent borreliacidal activity (50, 57, 58). Moreover, a veterinary vaccine consisting of chimeric OspC antigen combined with OspA

TABLE 1 *B. burgdorferi* OspC crystal structures and PDB codes

Type	Strain	PDB ID	Reference
A	B31	1GGQ	24
B	ZS7	7UJ2	This study
E	N40	1G5Z	85
I	HB19	1F1M	24
K	297	7UJ6	This study

proved effective at eliciting OspC antibodies and in preventing the onset of LD-like symptoms in dogs following experimental challenge with field-caught *B. burgdorferi*-infected ticks (56). In a separate line of investigation, Baum and colleagues examined human and mouse immune sera reactivity with a panel of 23 OspC types and delineated residues that determine type-specific cross-reactive antibody binding (41).

In recent years, the emergence of antibody- and structure-based approaches to vaccine design has accelerated the discovery of candidate vaccines for highly antigenically variable pathogens such as influenza virus, HIV-1, SARS-CoV-2, and even malaria (59–61). In effect, antigens are engineered around protective linear or conformational (discontinuous) epitopes defined by high-resolution X-ray and cryo-electron microscopy structures of antigen-antibody complexes. We reasoned that such an approach might be suited to OspC-based vaccine design. Indeed, the structures of three OspC types, A ($OspC_A$), I ($OspC_I$) and E ($OspC_E$), were solved more than 2 decades ago and shown to share a high degree of similarity (Table 1; see Fig. S1 in the supplemental material) (23, 24). OspC consists of four long α-helices (1–3, 6), two shorter α-helices (4 and 5), and two short antiparallel β-strands located between α1 and α2 (23, 24). The biologically functional molecule is a dimer (with monomers referred to here as OspC-OspC′) that assumes a knob-shaped structure anchored via an N-terminal lipidated moiety in the spirochete's outer membrane (23–25). While the structures of several OspA-antibody complexes have been solved and proved useful in next-generation OspA-based vaccine design (62–64), no OspC-antibody complexes have been reported.

B5 is an OspC-specific monoclonal IgG2a antibody (MAb) identified in a screen of B cell hybridomas derived from mice infected with *B. burgdorferi* strain B31 (OspC type A) (65). Passive immunization studies demonstrated that B5 IgG was sufficient to protect mice against experimental tick-mediated *B. burgdorferi* challenge, possibly by interfering with spirochete egress from the tick midgut (31, 66). Liang and colleagues also demonstrated that passive administration of B5 IgG was sufficient to protect mice against *B. burgdorferi* challenge by needle injection (67). B5 IgG is used widely as a reagent in the research community and, to our knowledge, remains the only OspC MAb to have been shown to be protective in a tick infection model of the natural route of *B. burgdorferi* transmission. Thus, we reasoned that deciphering the molecular interactions between B5 IgG and OspC will yield important information about mechanisms involved in blocking *B. burgdorferi* transmission to and dissemination within mammalian hosts.

RESULTS

B5 IgG was originally isolated from mice that had been experimentally challenged with *B. burgdorferi* strain B31 (31, 68). Due to a limited supply of hybridoma-derived mouse B5 IgG, we generated a recombinant chimeric derivative of B5 in which the murine V_H and V_L elements were fused to human IgG_1 Fc and kappa light chains, respectively, and expressed in Expi293 cells. We confirmed that mouse B5 IgG2a, as well as the chimeric derivative of B5 had reactivity with OspC. Recognition of native OspC on the surface of viable spirochetes was demonstrated by flow cytometry: *B. burgdorferi* strain B313, which endogenously overexpresses $OspC_A$, was incubated with B5 IgG or an isotype control (PB10 IgG) followed by Alexa 647-labeled secondary antibody and then analyzed for mean fluorescence intensity (MFI). B5 IgG labeled 70 to 80% of the live spirochetes with an MFI of $>$3200, compared to the isotype control, which labeled

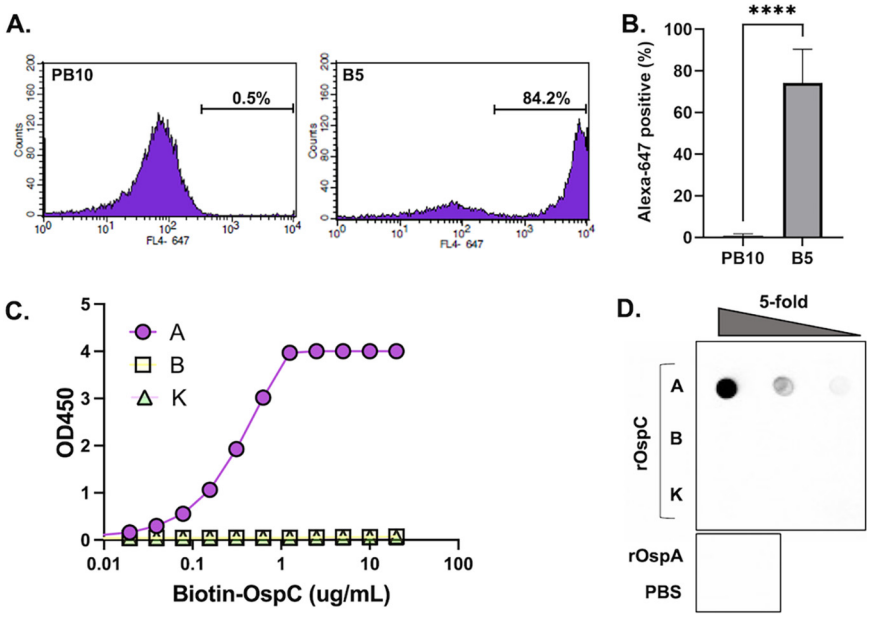

FIG 1 Reactivity of B5 IgG with native and recombinant OspC. (A and B). Mid-log phase *B. burgdorferi* overexpressing $OspC_A$ was incubated with chimeric B5 IgG or an isotype control (PB10) for 1 h at 37°C, washed, and then labeled with Alexa 647-labeled goat anti-human secondary antibody. Cells were analyzed using a BD FACSCalibur flow cytometer. Panel A shows a representative histogram of PB10 (left) and B5 (right) with relative fluorescence plotted on the *x* axis and the number of events plotted on the *y* axis. Panel B shows the total number of Alexa-positive cells following PB10 and B5 treatment from three independent replicates. Asterisks indicate statistical differences ($P < 0.001$) based on Student's *t* test. (C) Capture of biotin-tagged recombinant OspC types A, B, and K by immobilized B5 IgG, as described in Materials and Methods. The capture ELISA is representative of three independent replicates. (D) Reactivity of B5 IgG with 5-fold serial dilutions of recombinant OspC types A, B, and K spotted onto nitrocellulose membrane. Recombinant OspA (rOspA) and PBS were spotted as negative controls.

<1% of cells with an MFI of ~50 (Fig. 1A and B). To assess the breadth of B5 IgG reactivity, enzyme-linked immunosorbent assay (ELISA) plates were coated with recombinant $OspC_A$ and OspC type B ($OspC_B$) and K ($OspC_K$) and then probed with chimeric B5 IgG at a range of concentrations. By ELISA, B5 IgG reacted with $OspC_A$ but had no detectable reactivity with either $OspC_B$ or $OspC_K$ (Fig. 1C). Similar results were observed by dot blot analysis (Fig. 1D). Using biolayer interferometry (BLI), B5 IgG had an apparent dissociation constant (K_D) of ~0.2 nM for recombinant $OspC_A$ (Fig. S2). These results confirm that B5 recognizes both native and recombinant $OspC_A$ but has no measurable reactivity with $OspC_B$ or $OspC_K$.

B5 IgG epitope localization using hydrogen exchange-mass spectrometry (HX-MS). It was previously reported that B5 IgG recognizes a conformationally sensitive epitope involving the C terminus of α-helix 6 (68). To localize B5 IgG's epitope in more detail, recombinant homodimeric $OspC_A$ was subjected to HX-MS in the absence and presence of B5 IgG. HX-MS provides peptide-level resolution of antibody-antigen interactions in solution, based on differential hydrogen-deuterium exchange rates between unbound and bound targets (69–76). We recently used HX-MS to localize a dozen human B cell epitopes on the *B. burgdorferi* antigen OspA (77). In the case of OspC, we first generated a peptidic map of $OspC_A$, which yielded 87 peptides that covered the entire length of the molecule (Fig. S3). By HX-MS, the N- and C-terminal regions of OspC displayed a high degree of flexibility in the unbound state, as evidenced by a high degree of exchange (data not shown). The addition of B5 IgG resulted in weak, but statistically significant, protection across the majority of the OspC peptides, possibly reflecting a combination of allosteric effects and dynamic interconversion between bound and unbound states of the antigen. The strongest protection, however, encompassed α-helix 6, corresponding to $OspC_A$ peptidic residues 163 to 168, 171 to 172, 174 to 175, 177 to 179, 181 to 182, 184 to 186, 188 to 197, and 199 to 200 (Fig. 2). These

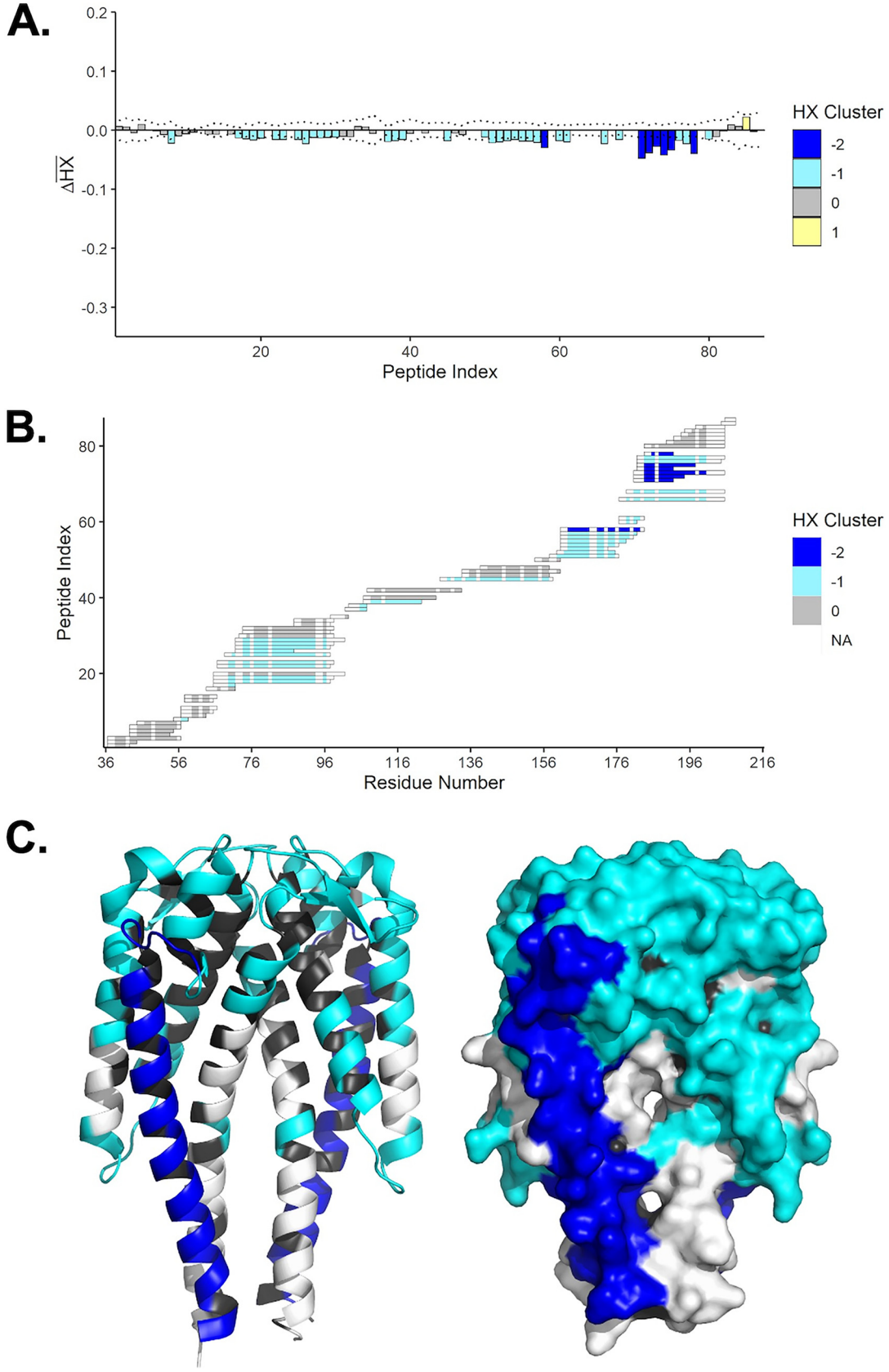

FIG 2 Localization of B5 IgG binding sites on $OspC_A$ by HX-MS. (A) Time-averaged, normalized HX differences (Δ*HX*) between $OspC_A$ and $OspC_A$ bound to B5 IgG. Negative bars denote slower HX in the presence of B5 IgG. The peptide index organizes

(Continued on next page)

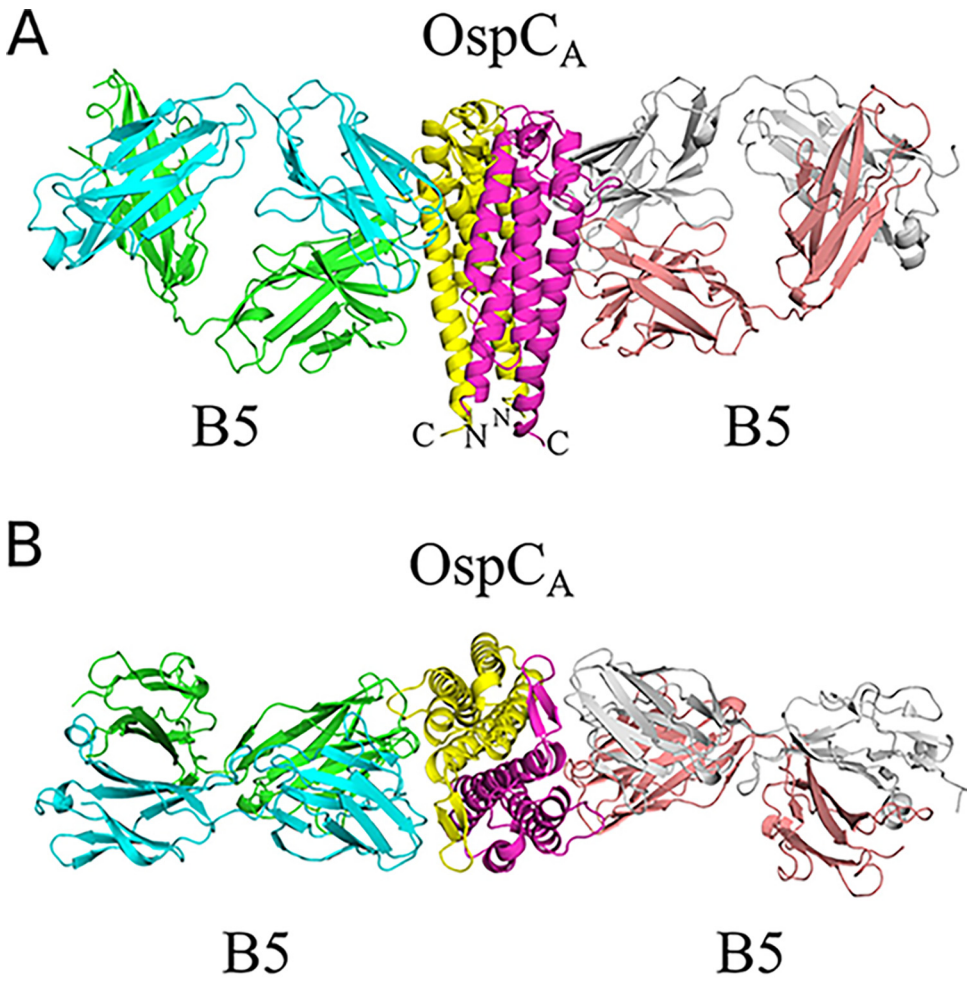

FIG 3 Structure of B5 Fab-OspC$_A$. (A and B) Side-on (A) and top-down (B) ribbon diagrams of OspC$_A$ homodimer (OspC$_A$, OspC$_A$′) in complex with B5 Fabs (B5, B5′). The OspC$_A$ is colored in yellow and OspC$_A$′ is magenta. The B5 Fab V_H and C_H1 elements are colored light green, and the V_L and C_L are cyan. The B5′ Fab V_H and C_H1 elements are colored in salmon red, and V_L and C_L are in light gray. The N- and C termini of OspC$_A$ and OspC$_A$′ are labeled accordingly (N, C).

results demonstrate that binding of B5 IgG influences the flexibility of the entire length of OspC's terminal α-helix, although HX-MS itself does not afford sufficient resolution to identify the actual antibody-antigen contact points.

X-ray crystal structure of Fab B5-OspC$_A$. To define B5's epitope in greater detail, we solved the X-ray crystal structure of the B5 Fab fragment in complex with OspC$_A$ at a 2.7-Å resolution in the $P2_12_12$ space group. The crystal structure revealed two B5 Fabs bound to a single OspC$_A$ homodimer (1:1 Fab:OspC$_A$ stoichiometry) in a side-on fashion (Fig. 3). The B5 Fab fragments (Fab, Fab′) made nearly identical contacts on opposite sides of the OspC$_A$ homodimer, as described in detail below. B5 Fabs assumed a canonical structure with two heavy-chain immunoglobulin domains (V_H, C_H1) and two light immunoglobulin domains (V_L, C_L), each containing seven to ten β-strands arranged in two β-sheets that folded into a two-layer sandwich with all six complementarity-determining regions (CDRs; L1-3, H1-3) on one face of the molecule. The homodimeric

FIG 2 Legend (Continued)
the peptides from the N to C termini. The values are color-coded based on k-means clustering. Extreme cluster values (e.g., −2) denote stronger effects. (B) Peptide resolution map of the B5 IgG epitope showing clustered HX; (C) Cartoon (left) and surface (right) representations of OspC$_A$ [PDB ID 1GGQ] with relative effects of B5 IgG as interpreted from panels A and B. The dark blue shading represents strongly protected regions of OspC$_A$, light blue represents weak (but significant) protection, and black denotes lack of coverage.

TABLE 2 Summary of $OspC_A$-B5 binding data and interface information

Interface	H-bonds[a]	Salt bridges	Shape comp.[b]	BSA (Å^2)
1°	9	3	0.68	2,040
2°[c]	12	3	0.61	2,002

[a]Hydrogen bonds.
[b]Shape complementarity score.
[c]Second RTA-V_HH complex in crystallographic asymmetric unit.

structures of $OspC_A$ unbound (PDB 1GGQ) and bound to B5 Fabs were similar, as evidenced by a root-mean-square deviation (RMSD) of 1.0 Å for all atoms. Thus, antibody engagement did not induce any major conformational changes in $OspC_A$.

The interaction between B5 Fab and $OspC_A$ buried a total surface area of 2,040 Å^2 (2,002 Å^2 for the second B5-$OspC_A$ interface within the asymmetric unit) establishing 9 hydrogen bonds and 3 salt bridges (12 hydrogen bonds and 3 salt bridges for the second B5-$OspC_A$ interface within the asymmetric unit) (Table 2; Fig. 4). The B5 Fab V_H domain contributed slightly more to the interaction, burying 1,042 Å^2 (1,027 Å^2 for the second B5-$OspC_A$ contact within the asymmetric unit) more than the V_L domain, which buried 998 Å^2 (975 Å^2 for the second B5-$OspC_A$ interface in the asymmetric unit). The

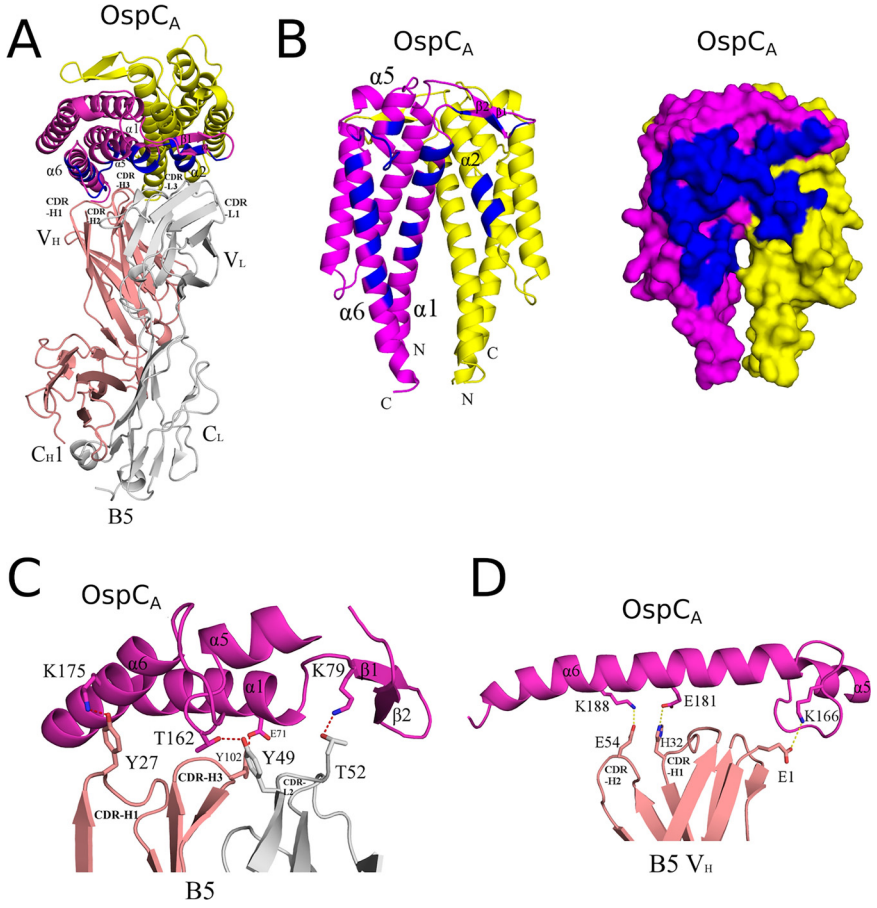

FIG 4 Detailed interactions between B5 and $OspC_A$ revealed from the cocrystal structure. (A) Ribbon structure (top-down view) of the $OspC_A$ homodimer ($OspC_A$, magenta; $OspC_A'$, yellow) in complex with a single B5 Fab (V_H and C_H1 elements, salmon red; V_L and C_L, light gray). The $OspC_A$ residues that engage with B5 are colored blue. Key secondary structures are labeled (α-helices 1, 2, 5, and 6; β-strands 1 and 2). (B) Ribbon (left) and surface (right) depiction of an $OspC_A$ homodimer ($OspC_A$, magenta; $OspC_A'$, yellow) with B5 interacting residues shaded in dark blue. $OspC_A$ N and C termini are labeled N and C, respectively. (C and D) Representations of key (C) H-bonds (red dashes) and (D) salt bridges (yellow dashes) between $OspC_A$ (magenta) and Fab B5 (salmon and gray in panel C; gray in panel D). Side chains are drawn as sticks and color coordinated to the main chain color, with nitrogen atoms shaded blue and oxygen atoms shaded red. CDR elements are labeled per convention: CDR-L1, -L2, -L3; CDR-H1, -H2, -H3.

B5 V_H domain formed four hydrogen bonds (three hydrogen bonds for the second B5-$OspC_A$ interface in the asymmetric unit), including CDR-H1 residue Tyr-27 with $OspC_A$ Lys-175 and CDR-H3 residue Tyr-102 and $OspC_A$ Glu-71 (Fig. 4). The B5 V_H domain also accounted for two of the three salt bridges observed between B5 and $OspC_A$. The two salt bridges formed between B5's V_H domain and $OspC_A$ involved H2 Glu-54 with $OspC_A$'s Lys-188 and H1 His-32 with Glu-181. The third salt bridge involved V_H framework residues Glu-1 and $OspC_A$ Lys-166 (Fig. 4). The B5 V_L domain formed five hydrogen bonds (eight hydrogen bonds for the second B5-$OspC_A$ interface within the asymmetric unit), including CDR L2 Thr-52 with $OspC_A$ Lys-79, and CDR L2 Tyr-49 with $OspC_A$ Thr-162. There were no salt bridges between the B5 V_L domain and $OspC_A$.

Collectively, the B5 CDR H1, H2, and H3 elements contacted $OspC_A$ α-helix 1 and α-helix 6, along with the loop between α-helices 5 and 6 (loop 5-6). The CDR H3 element also buried 30 Å^2 of α-helix 2′ in the absence of any H-bonds or salt bridges. CDRs L1, L2, and L3 contacted $OspC_A$ α-helices 1 and 5, β-strands 1 and 2, and the loop region immediately N-terminal to α-helix 6. CDR L1 and L3 interacted with α-helix 2′, burying 364 Å^2 and forming a single H-bond between CDR L1 Asn-30 and Gln-110 in $OspC_A$. The fact that B5 Fabs straddle the OspC dimer interface not only explains the conformation-dependent nature of B5's epitope, but more broadly explains the observation that immunizing mice with homodimeric OspC is more effective than monomeric OspC at eliciting protective antibodies (37).

Structural basis of B5 IgG specificity for $OspC_A$. To elucidate the structural basis for B5 IgG's specificity for $OspC_A$, we solved the crystal structures of recombinant $OspC_B$ and $OspC_K$ at 1.5-Å and 1.9-Å resolution, respectively, in the $P2_1$ space group (Fig. S4). $OspC_B$ and $OspC_K$ each formed homodimers nearly identical to those of $OspC_A$ (unbound or bound to B5). Specifically, $OspC_B$ and $OspC_K$ monomers each consisted of four long α-helices (1–3, 6), two shorter α-helices (4 and 5), and a two-stranded β-sheet (Fig. S4). The RMSD between the homodimeric $OspC_A$ (bound to B5) versus $OspC_B$ and $OspC_K$ ranged from 0.8 Å to 1.4 Å for all atoms. In each case, the OspC dimer interface is predominantly hydrophobic, with ~80% of the protein atoms in the interface being nonpolar. The monomeric form of $OspC_A$ (with or without B5 Fab bound) was structurally more similar to $OspC_K$ than $OspC_B$, with an RMSD of ~0.7 Å for all atoms. A deletion at residue 74 and an insertion of residue 165 in $OspC_B$ relative to $OspC_A$ and $OspC_K$ accounts for the greater structural deviation of $OspC_B$ to $OspC_A$ and $OspC_K$, as exhibited by an RMSD of 0.9 Å for all atoms when the $OspC_B$ monomer was superposed onto $OspC_A$ or $OspC_K$ monomers. More specifically, atoms in $OspC_B$ residues 70 to 75 and 160 to 168 were the most structurally different, with RMSDs of 1.4 Å and 1.9 Å, respectively, compared to the analogous regions in $OspC_A$ and $OspC_B$. After molecular replacement calculations were performed, the resulting phase information was used to calculate electron density maps utilized to manually insert the correct residues into each model and manually build other regions of each model for the $OspC_B$ and $OspC_K$ structures. Crystallographic and refinement data for each structure demonstrated a refined molecular model with excellent agreement to the crystallographic data, as well as excellent geometry. B5 V_H residues Arg-67 and Ser-77, which have well-defined electron density, are the only two Ramachandran plot outliers (Table S1).

Superpositioning the B5-$OspC_A$ complex onto $OspC_B$ and $OspC_K$ revealed additional structural attributes that likely account for B5's inability to recognize $OspC_B$ and $OspC_K$. One prominent feature involves the contact between B5 Trp-100 with Gly-174 in $OspC_A$. In $OspC_B$ and $OspC_K$, Glu-175 is superposed with $OspC_A$ Gly-174. The bulkier and negatively charged Glu-175 side would be expected to clash (sterically and electrostatically) with Trp-100, thereby impeding B5 interaction (Fig. 5A; Fig. S5). Furthermore, in the case of $OspC_B$, an "insertion" of Ala-162 within loop 5-6 relative to $OspC_A$ alters the configuration of the loop, resulting in a theoretical clash of B5 with Tyr-47 (Fig. 5B; Fig. S5). $OspC_B$ is also unable to H-bond with B5 Tyr-47, due to an Ala rather than a Thr at position 162, as is the case in $OspC_A$. The absence of this H-bond donor would be expected to compromise the B5-

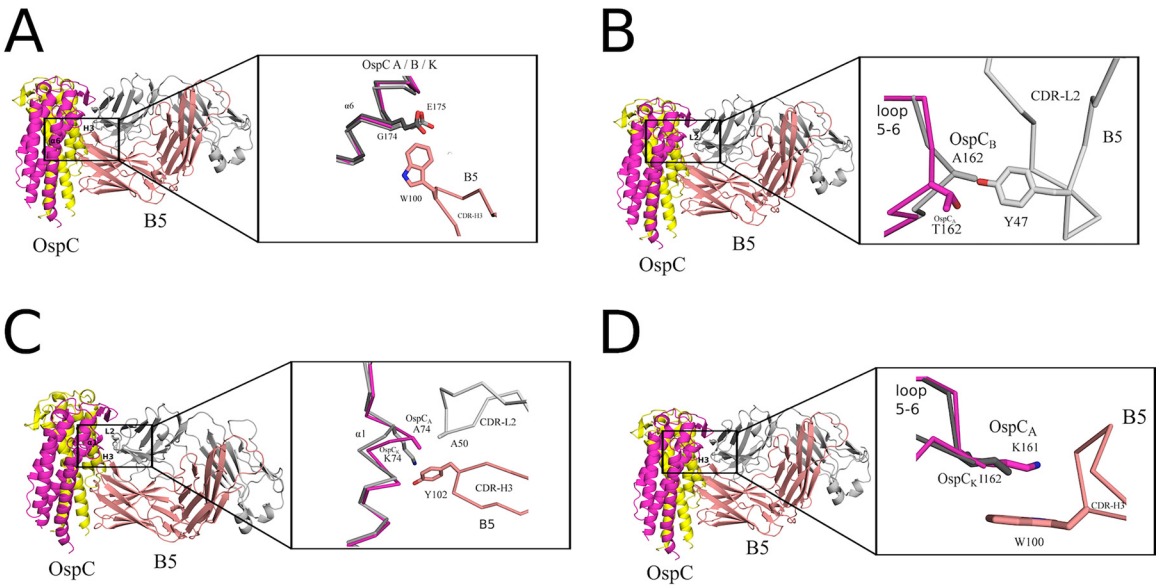

FIG 5 Structural basis of B5 specificity for OspC$_A$. Interface between B5 Fab and OspC$_A$ superposed with OspC$_B$ and OspC$_K$ highlighting the key residues in OspC$_B$ and Osp$_K$ that conceivably disrupt interaction with B5. (A) A zoom-out view of the ribbon diagram of the OspC-B5 complex and a zoom-in view of the C-α traces of OspC$_A$ (magenta) bound to B5 (salmon red) with superposed OspC$_B$ (light gray) and OspC$_K$ (dark gray) highlighting potential electrostatic and steric clash between Glu-175 of OspC$_B$ and OspC$_K$ with Trp-100 of B5 Fab. (B) The OspC-B5 ribbon diagram with a closeup of the C-α traces of OspC$_A$ (magenta) bound to B5 (salmon red) superposed with OspC$_B$ (light gray). The image highlights likely repulsion between Ala-162 of OspC$_B$ with Tyr-49 of B5 Fab. (C) A zoom-out view of the OspC-B5 complex as a ribbon diagram and a zoom-in perspective of the C-α traces of OspC$_A$ (magenta) bound to B5 with CDR-H3 (salmon red) and CDR-L2 (gray) superposed with OspC$_k$ (light gray). The image highlights a potential clash between Lys-74 of OspC$_K$ and B5's Tyr-102. (D) The ribbon diagram of the OspC-B5 complex and a closeup of the C-α trace of OspC$_A$ (magenta) bound to B5 (salmon red) superposed with OspC$_K$ (dark gray). Ile-162 in OspC$_k$ precludes a potential π-cation interaction that occurs between OspC$_A$ Lys-161 and Trp-100 in B5 Fab. All ribbon diagrams of the OspC-B5 complex are drawn with the OspC dimer colored yellow and magenta. The B5 Fab heavy chain is colored salmon red with the light chain colored light gray. Side chains are drawn as sticks and color coordinated to the main chain color, with nitrogen atoms shaded blue and oxygen atoms shaded red.

OspC$_B$ interaction. Another structural feature in OspC$_B$ disfavoring B5 binding includes deletion of one residue immediately before Lys-74 in OspC$_B$. This deletion substantially altered residue positions 73 to 75 within α-helix 1 of OspC$_B$ relative to the same residues in OspC$_A$ and OspC$_K$. As a result, the superposed side chain of Lys-74 in OspC$_B$ clashes with B5 Tyr-102. Though several preferred rotamers of OspC$_B$ Lys-74 can readily pivot away from B5 Tyr-102, alleviating the close encounter between these two residues, movement of Lys-74 away from Tyr-102 and B5 residue Ala-50 would significantly reduce contact between B5 and OspC$_B$ by $\sim$50 Å^2, likely diminishing B5 binding to OspC$_B$ (Fig. 5C; Fig. S5). In the case of OspC$_K$, divergent primary amino acid sequences at consequential residues further contributed to a lack of B5 recognition. For example, OspC$_A$ Lys161 forms a π-cation interaction with B5 Trp-100, which cannot occur in the case of OspC$_K$ due to an Ile residue at this position (Fig. 5D; Fig. S5). To determine the potential cross-reactivity of B5 with the other OspC types, we examined primary sequence conservation across each OspC, focusing on regions in OspC$_A$ that support B5 binding while also considering regions in OspC$_B$ and OspC$_K$ that seemingly antagonize B5 interaction. We predict that two OspC types, C3 and I3, with 76% and 78% overall sequence identities to OspC$_A$, respectively, would interact with B5. C3 and I3 possess similar sequences within α-helix 1 and loop 5-6 along with a few other key B5 contact residues found in OspC$_A$ (Fig. S6). For example, OspC$_{I3}$ is similar to OspC$_A$ in that it has a Gly at position 174, providing ample room to contact B5's Trp-100. In the case of OspC$_{C3}$, an Asp residue replaces Gly-174; while the Asp side chain is larger than that of Gly, there is still sufficient space to engage Trp-100 in B5. It is interesting that Baum and colleagues demonstrated experimentally that OspC$_A$ and OspC$_{I3}$ were the most immunologically cross-reactive pairs in a protein microarray consisting of 23 OspC types (41). Structural insights into the

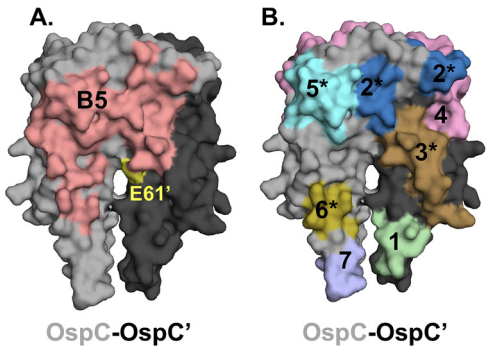

FIG 6 Depiction of functional residues and linear human B cell epitopes and B5 contact points on the OspC homodimer. Surface representation of the $OspC_A$ homodimer (PDB 1GGQ) with one monomer colored light gray (OspC) and the other charcoal (OspC′). (A) Depiction of B5's "footprint" (salmon red) on the OspC dimer. Residue E61 (see the text for details) on OspC′ is colored in yellow. (B) Seven (1 to 7) reported linear B cell epitopes on OspC, as detailed in Table 3. The asterisks (*) indicate linear epitopes that are predicted to fall within B5's epitope.

molecular interactions that promote or repel protective antibodies has important implications for rational vaccine design.

Location of functional residues and human linear B cell epitopes on OspC relative to B5's binding site. OspC is a multifunctional protein that interacts with substrates in both the vector (e.g., Salp15) and mammalian hosts (e.g., plasminogen, C4b) (5). While the exact residues on OspC involved in these interactions have not been elucidated, Eicken and others described a putative ligand binding domain (LBD1) situated at the dimer interface (Fig. 6A) (23). Earnhart and colleagues demonstrated that a point mutation in Glu-61 (E61Q) in proximity to LBD1 of $OspC_A$ rendered *B. burgdorferi* strain B31 noninfectious in a mouse model of needle (subcutaneous) challenge (51). We used PyMol to visualize the location of the $OspC_A$ E61 relative to B5's epitope, with the idea that occlusion of this residue by B5 might account for B5's functional activity *in vivo* (Fig. 6A). While the interface between B5 Fab and Lys-60, Glu-61, and Glu-63 within LBD1 is minimal (37 $Å^2$ in first asymmetric unit; 25 $Å^2$ in the second asymmetric unit), B5 V_H residues nonetheless engage two residues (Lys-60 and Ala-64) on opposing sides of the LBD1 cavity, as defined by Earnhart and colleagues (51). For that reason, we cannot rule out the possibility that B5 IgG does in fact limit LBD1 ligand accessibility.

To put B5's epitope in context with other known landmarks on OspC, we extracted the seven human linear B cell epitopes on OspC from the Immune Epitope Database (IEDB.org) (Table 3) and mapped them, using PyMol, onto the crystal structure of dimeric $OspC_A$ (Table 3; Fig. 6B). Four of the seven linear epitopes (no. 2, 3, 5, 6) are predicted to fall within B5's binding site, revealing an overlap between B5's epitope and known human B cell epitopes on OspC. However, functional activities have not been ascribed to any of these four linear epitopes to date, so we can only speculate as to the impact of antibody occupancy on OspC activity *in vivo*. The two linear B cell epi-

TABLE 3 Human linear B cell epitopes on OspC and putative overlap with B5 contact points

No.	Residues[a]	Sequence	B5[b]	IEDB ID[c]	Reference
1	38–53	KGPNLVEISKKITDSN	−	559957	96
2	71–86	EIAAKAIGKKIHQNNG	+	12383	97
3	104–118	ISTLIKQKLDGLKNE	+	28749	97
4	130–150	CSETFTNKLKEKHTDLGKEGV	−	6984	98
5	156–171	AKKAILITDAAKDKG	+	181187	99
6	184–190	LKAAKEM	+	560173	96
7	195–210[b]	PVVAESPKKP	−	49993	100

[a]Sequences from OspC type A (strain B31), except 5 from $OspC_K$.
[b]+, Spatial overlap with B5's epitope; –, No overlap with B5.
[c]The Immune Epitope Database (IEDB) unique identified number. The underlined numbers in the first column (far left) indicate an epitope associated with borreliacidal activity.

topes (no. 4, 7) on OspC that have been associated with complement-dependent borreliacidal activity are outside of B5's footprint (Table 3; Fig. 6B).

DISCUSSION

OspC has long been considered a prime LD vaccine antigen due to its vital role in *B. burgdorferi* pathogenesis, coupled with the fact that it is a target of protective antibodies capable of interfering with both tick-mediated transmission and early stages of mammalian infection (11). Indeed, recombinant (chimeric) antigens with concatenated linear B cell epitopes from different OspC types have proven to be effective veterinary vaccines and may have applications to humans (13, 53). However, linear B cell epitopes constitute only one facet of the antibody response to OspC. There is considerable evidence that conformation-dependent epitopes on OspC are essential in eliciting protection against *B. burgdorferi* experimental challenge via tick bite and needle injection (37, 68). Despite this fact, a high-resolution map of discontinuous protective and nonprotective B cell epitopes on OspC is lacking.

In this study, we report the first structure of a protective B cell epitope on OspC, as defined by the mouse monoclonal antibody, B5. B5 is the only OspC-specific monoclonal antibody to have been shown to passively protect mice against both needle- and tick-mediated *B. burgdorferi* infection (31, 78, 79). The B5 Fab-$OspC_A$ structure is notable in several respects. First, the structure reveals that B5 attacks the $OspC_A$ homodimer at a right angle, favoring an interaction with OspC's stem (α-helices 1 and 6), rather than the more accessible head (24). While the significance of this side-on orientation is currently unknown, it does result in at least partial occlusion of OspC's LBD1, which includes residues implicated in *B. burgdorferi* infectivity of mice (51). Whether occlusion of LBD1 is related to B5 IgG's ability to limit dissemination of *B. burgdorferi* in the mouse model remains to be determined.

Second, the B5 Fab-$OspC_A$ structure reveals that B5's epitope is quaternary, as the V_H and V_L elements span the OspC-OspC′ dimer interface (Fig. 4B). This observation reaffirms the notion that OspC exists as a dimer on the surface of *B. burgdorferi*, because B5 IgG was isolated from mice that had been infected by tick-bite with viable spirochetes (31, 65). It also explains, at least in part, why monomeric OspC is significantly less effective than dimeric OspC at simulating protective immunity (37). Selection and affinity maturation of B5-like antibodies would only arise in the presence of OspC homodimers in which the OspC-OspC′ interface is preserved. This fact has obvious implications for OspC-based subunit vaccines, as alluded to by others (37). Finally, B5 adds to the growing list of protective monoclonal antibodies that target quaternary epitopes, including on AB toxins (80) and viruses such as Ebola (81) and SARS-CoV-2 (82).

In an effort to define the molecular basis of B5's specificity for $OspC_A$, we also solved the crystal structures of dimeric OspC types B and K (Table 1). The addition of $OspC_B$ and $OspC_K$ to the list of available structures is significant because *B. burgdorferi* invasive strains are primarily associated with OspC types A, B, I, and K (42–44). Having all four OspC structures publicly available will enable them to be used for computational-based design of broadly reactive vaccine antigens following a playbook similar that used for influenza virus (83). As predicted, the overall tertiary and quaternary structures of $OspC_B$ and $OspC_K$ are similar to each other and to the other available OspC structures. Nonetheless, we identified both primary and secondary elements on OspC that likely account for B5 recognition of $OspC_A$, but not $OspC_B$ or $OspC_K$. Unfortunately, the inclusion of computational modeling to assess B5-OspC dynamics and reactivity with other OspC types was beyond the scope of the current study.

As a final note, it is worth pointing out that Eicken and colleagues commented on the similarity of the structure of OspC to that of the variable surface glycoprotein (VSG) from *Trypanosoma brucei* (84, 85). Twenty years later this parallel can be extended to include comparisons between B5-OspC and VSG-antibody complexes. A recent report describes the structures of three llama-derived single-domain antibodies (nanobodies or VHHs), including one with potent activity against living parasites, including arresting trypanosome motility and promoting membrane blebs (86). Reminiscent of the B5-OspC structure, the authors found that the three nanobodies engage VSG at a right angle near

the base of the molecule rather than the head, where they had predicted. Interestingly, the authors argue that engagement with VSG in this orientation has profound effects on trypanosome membrane flexibility, which ultimately impairs the parasite's motility. A similar mechanism could be at play in the case of B5 and OspC. Occupancy of the lateral face of OspC would be expected to perturb higher-order OspC oligomers or lattices on the bacterial surface, which have been alluded to in the literature (23). Alternatively, B5 might perturb overall membrane fluidity and lipid raft formation critical to *B. burgdorferi* pathogenesis (87). In theory, any given antibody bound to OspC would be expected to affect OspC fluidity in the spirochete membrane. However, not all OspC monoclonal antibodies are protective (37), so other factors such as epitope specificity may be at play. Sorting out the antibody determinants that influence the outcome between *B. burgdorferi* and host infectivity ultimately will inform a next-generation LD vaccine.

MATERIALS AND METHODS

Mouse and chimeric B5 IgG MAbs. Lyophilized B5 IgG from the CDC was reconstituted to final concentration of 6 mg/mL. B5 Fab fragments were generated by papain digestion followed by affinity depletion of the Fc fragment by protein A fast protein liquid chromatography (FPLC). The resulting B5 Fab was purified to homogeneity by size exclusion chromatography (SEC) using a Superdex 200 16/60 gel filtration column. The B5 mouse hybridoma was cultured as described previously from frozen aliquot (31). In addition, to ensure sufficient supply of B5 MAb, the mouse B5 V_H and V_L regions were cloned into human IgG1 Fc and κ light chain expression vectors and used to transfect Expi293 cells following protocols previously described (88). The resulting chimeric B5 IgG1 was purified and used for dot blot and flow cytometry analysis.

Affinity measurement using biolayer interferometry (BLI). Biotinylated $OspC_A$ (3 μg/mL) in buffer (phosphate-buffered saline [PBS] containing 2% wt/vol bovine serum albumin [BSA]) was captured onto streptavidin biosensors (no. 18-5019, Sartorius, Göttingen, Germany) for 5 min. After 3 min of baseline in buffer, sensors were then exposed to a 2-fold serial dilution of MAb B5, ranging from 100 to 1.56 nM, for 5 min. The sensors were then dipped into wells containing buffer alone for 30 min. An eighth sensor was also loaded with biotinylated-$OspC_A$, but not exposed to MAb B5, and was thus used as a background drift control and subtracted from the other sensor data. The raw sensor data were then loaded into the Data Analysis HT 12.0 software, and the data were fit to a 1:2 bivalent analyte model. Data were captured on an Octet RED96e biolayer interferometer (Sartorius) using the Data Acquisition 12.0 software.

Indirect fluorescent antibody staining and flow cytometry. B313, a derivative of *B. burgdorferi* strain B31 that endogenously expresses $OspC_A$ as described by Sadziene et al. (89) was kindly provided by Yi-Pin Lin (Wadsworth Center). The strain was cultured in BSK-II medium at 37°C with 5% CO_2 to mid-log phase. Cells were collected by centrifugation (3,300 $\times$ *g*), washed with PBS, resuspended in BSK-II (minus phenol red indicator) at a final concentration of 1×10^8 cells/mL, and incubated at room temperature for 30 min. A total of 5×10^6 cells in 50 μL were incubated with 10 μg/mL of chimeric B5 IgG1 at 37°C for 1 h. Incubation with an isotype control, PB10, was included as a negative control (90). The reaction volume was then increased with the addition of 450 μL of BSK-II (minus phenol red), and goat anti-human IgG [H+L]-Alexa 647 (Invitrogen) was added at a 1:500 dilution and allowed to incubate at 37°C for 30 min. Alexa-647-labeled cells were analyzed on a BD FACSCalibur flow cytometer. Data were obtained and analyzed using BD's CellQuest Pro software.

Dot blot analysis. Recombinant OspC types A, B, and K (Table 1) at 0.5 μg/μL, were 5-fold serially diluted in PBS, and 2 μL of each dilution was spotted on a dry nitrocellulose membrane. The spots were allowed to air dry for 1 h and then were blocked with 5% milk in 1$\times$ Tris-buffered saline with Tween 20 (TBS-T) for 18 h and incubated with 0.1 μg/mL chimeric B5 IgG1 in 5% milk in 1$\times$ TBS-T at room temperature for 1 h. The membrane was then washed twice with 1$\times$ TBS-T, incubated with a 1:10,000 dilution of goat anti-human IgG (H+L)-horseradish peroxidase (HRP; Invitrogen), and washed twice more before detection with enhanced chemiluminescence (ECL; ECL Plus Western blotting substrate; Pierce, Thermo Fisher, Waltham, MA). Images were acquired and analyzed using an iBright 1500 system (Invitrogen).

OspC ELISA. B5 IgG was coated onto wells of a 96-well Immulon 4HBX plate (Thermo Fisher, Waltham, MA) at 1 μg/mL in PBS overnight at 4°C. Wells were then blocked for 2 h at room temperature with 2% goat serum in 0.1% Tween 20 in PBS. Biotinylated OspC types A, B, and K were then diluted 2-fold across the plate, starting at 20 μg/mL. Plates were washed, and then captured biotinylated OspC was detected with avidin-HRP (Pierce, Rockford, IL) for 1 h. Plates were washed again, and capture was visualized with SureBlue *N*,*N*,*N*′,*N*′-tetramethyl-1,3-butanediamine (TMB; SeraCare, Milford, MA). The reaction was stopped with 1 M phosphoric acid, and the optical density at 450 nm was read using a SpectraMax iD3 instrument (Molecular Devices, San Jose, CA).

Liquid chromatography-mass spectrometry (LC-MS) analysis. For peptic peptide mapping, recombinant $OspC_A$ was diluted with quench solution (200 mM glycine, pH 2.5), and 50 pmol of sample was injected in each run. $OspC_A$ was digested by an in-house-prepared immobilized pepsin column (2.1 by 50 mm) (91). Digested peptides were trapped and desalted by C_8 (Zorbax 300SB C_8, 2.1 by 12.5 mm, 5-μm particles) for 120 s and separated by a C_{18} column (Zorbax 300SB 2.1 by 50 mm, 3.5 μm particle diameter, Agilent, Santa Clara, CA). For LC, mobile phase A was 0.1% formic acid in water, and B was 0.1% formic acid in acetonitrile. A total of a 25-min LC method was used: 10 min with 15% to 35% B was used to separate

peptides, and 15 min was used for cleaning purposes. Peptides were detected, and the mass was measured with a quadruple time of flight (Q-TOF) mass spectrometer (Agilent 6530 in electrospray ionization (ESI)-positive ion mode). All the peptic peptides were assigned by tandem mass spectrometry (collision induced dissociation [CID] fragmentation). Agilent MassHunter Qualitative Analysis with BioConfirm (version B.07.00) software was used for the analysis of all the mass spectrometry data. A total of 87 peptides were identified and mapped as shown in Fig. S1. This map shows 100% $OspC_A$ sequence coverage with a median length of 17.0 residues and 8.6 average redundancy.

Hydrogen exchange-mass spectrometry (HX-MS) and data analysis. $OspC_A$ and B5 MAb were buffer exchanged and assayed using our previous protocol (77). Previously flash-frozen $OspC_A$ (19 μM) was thawed at room temperature. B5 sample was collated from 4°C and buffer exchanged on the day of experiment. Free the protein state ($OspC_A$), sample was prepared by diluting 19 μM $OspC_A$ to 9 μM by the addition of 20 mM phosphate and 100 mM NaCl, pH 7.40. The bound state ($OspC_A$ +B5) was prepared by three strokes of mixing and adjusted to a final concentration of 9 μM. HX-MS labeling conditions, robot methods, maximally deuterated experiment (OspA paper) protocol, and data analysis were done as recently reported (77).

Cloning, expression, and purification of OspC. The PCR amplicon encoding *B. burgdorferi* $OspC_A$ (residues 38 to 201) was subcloned into the pSUMO expression vector that contained an N-terminal deca-histidine and SUMO tag. The PCR amplicons for *B. burgdorferi* $OspC_B$ and $OspC_K$ containing residues 38 to 202 were subcloned into the pMCSG7 expression vector that contained an N-terminal deca-histidine tag. Cloning was performed using standard ligase-independent cloning (LIC). All OspC types were expressed in *Escherichia coli* strain BL21(DE3). The transformed bacteria were grown at 37°C in TB medium and induced at 20°C at an optical density at 600 nm (OD_{600}) of 0.6 with 0.1 mM isopropyl-β-D-thiogalactopyranoside (IPTG) for ~16 h. After induction, cells were harvested and resuspended in 20 mM HEPES (pH 7.5) and 150 mM NaCl. The cell suspension was sonicated and centrifuged at 30,000 $\times$ *g* for 30 min. After centrifugation, the protein-containing supernatant was purified by nickel-affinity and size exclusion chromatography on an AKTAxpress system (GE Healthcare), which consisted of a 1-mL nickel affinity column followed by a Superdex 200 16/60 gel filtration column. The elution buffer consisted of 0.5 M imidazole in binding buffer, and the gel filtration buffer consisted of 20 mM HEPES (pH 7.5), 150 mM NaCl, and 20 mM imidazole. Fractions containing each OspC type were pooled and subjected to tobacco etch virus (TEV) protease cleavage (1:10 weight ratio) for 3 h at room temperature to remove the respective fusion protein tags. The cleaved proteins were passed over a 1-mL Ni-NTA agarose (Qiagen) gravity column to remove TEV protease, cleaved residues, and uncleaved fusion protein. After purification, Fab B5 was complexed with $OspC_A$ in a 1:1 stoichiometry and then concentrated to 10 mg/mL final for all crystallization trials.

Crystallization and data collection. All crystals were grown by sitting drop vapor diffusion using a protein to reservoir volume ratio of 1:1 with total drop volumes of 0.2 μL. Crystals of the B5 Fab-$OspC_A$ complex were produced at 22°C using a crystallization solution containing 100 mM sodium cacodylate, pH 6.5, 5% polyethylene glycol (PEG) 8K, and 40% Hexylene glycol (MPD). Crystals of the $OspC_B$ were produced at 22°C using a crystallization solution containing 100 mM sodium phosphate citrate, pH 4.2; 41.9% PEG 600 crystals of the $OspC_K$ were produced at 4°C using a crystallization solution containing 100 mM Tris, pH 8.5, 40% PEG 400, 200 mM LiSO4, and 10 mM 2-aminoethanesulfonic acid. All crystals were flash-frozen in liquid nitrogen after a short soak in the appropriate crystallization buffers supplemented with 25% ethylene glycol. Data were collected at the 24-ID-E beamline at the Advanced Photon Source, Argonne National Labs. All data were indexed, merged, and scaled using HKL2000 (92) and then converted to structure factor amplitudes using CCP4 (93).

Structure determination and refinement. The B5 Fab-$OspC_A$ complex, $OspC_B$, and $OspC_K$ structures were solved by molecular replacement using Phaser (92). Molecular replacement calculations were performed using the coordinates of the murine monoclonal Fab 3E6 V_H and C_H1 domains (PDB ID: 4KI5) along with the V_L and C_L domains of the human germ line antibody hepatitis E virus E2S antibody (PDB ID: 3RKD) as the search model for Fab B5 in the B5-$OspC_A$ complex. The OspC coordinates (PDB ID: 1GGQ) were used as the search model for $OspC_A$ in the $OspC_A$-B5 complex. The same OspC coordinates (PDB ID: 1GGQ) were also used as search models for the $OspC_B$ and $OspC_K$ structure determinations. The resulting phase information from molecular replacement was used for some manual model building of each structure solved using the graphics program Coot (94) and structural refinement employing the PHENIX package (95). Data collection and refinement statistics are listed in Table S1, as are the Protein Data Bank (https://www.rcsb.org/) codes associated with each of the three structures generated in this study (B5-$OspC_A$, PDB ID 7UIJ; $OspC_B$, PDB ID 7UJ2; $OspC_K$, PDB ID 7UJ6). Molecular graphics were prepared using PyMOL (Schrodinger, DeLano Scientific LLC, Palo Alto, CA). All buried surface area calculations were done with PISA within the CCP4 suite (93).

SUPPLEMENTAL MATERIAL

Supplemental material is available online only.

FIG S1, PDF file, 0.3 MB.

FIG S2, PDF file, 0.03 MB.

FIG S3, PDF file, 0.1 MB.

FIG S4, PDF file, 0.3 MB.

FIG S5, PDF file, 0.3 MB.

FIG S6, PDF file, 1.4 MB.

TABLE S1, PDF file, 0.2 MB.

ACKNOWLEDGMENTS

We gratefully acknowledge the Wadsworth Center's Tissue and Cell culture facility for preparing BSK II medium and Renjie Song in the Immunology Core for assistance with flow cytometry. We thank Timothy LaRocca (Albany College of Pharmacy and Health Sciences) and Graham Willsey for insightful discussions and assistance. We thank Elizabeth Cavosie for administrative assistance.

This work was supported by the National Institute of Allergy and Infectious Diseases (NIAID), National Institutes of Health, Department of Health and Human Services contract no. 75N93019C00040. This work is based upon research conducted at the Northeastern Collaborative Access Team beamlines, which are funded by the National Institute of General Medical Sciences from the National Institutes of Health (P30 GM124165). The Eiger 16M detector on the 24-ID-E beam line is funded by an NIH-ORIP HEI grant (S10OD021527). The views are those of the authors and do not necessarily reflect those of the Centers for Disease Control and Prevention.

N.J.M. dedicates this article to the late Ronald Limberger for his contribution to the world of spirochetes and his leadership at the Wadsworth Center.

REFERENCES

1. Radolf JD, Strle K, Lemieux JE, Strle F. 2021. Lyme disease in humans. Curr Issues Mol Biol 42:333–384. https://doi.org/10.21775/cimb.042.333.
2. Steere AC, Strle F, Wormser GP, Hu LT, Branda JA, Hovius JW, Li X, Mead PS. 2016. Lyme borreliosis. Nat Rev Dis Primers 2:16090. https://doi.org/10.1038/nrdp.2016.90.
3. Burgdorfer W, Barbour AG, Hayes SF, Benach JL, Grunwaldt E, Davis JP. 1982. Lyme disease: a tick-borne spirochetosis? Science 216:1317–1319. https://doi.org/10.1126/science.7043737.
4. Barbour AG, Gupta RS. 2021. The family Borreliaceae (Spirochaetales), a diverse group in two genera of tick-borne spirochetes of mammals, birds, and reptiles. J Med Entomol 58:1513–1524. https://doi.org/10.1093/jme/tjab055.
5. Caine JA, Coburn J. 2016. Multifunctional and redundant roles of Borrelia burgdorferi outer surface proteins in tissue adhesion, colonization, and complement evasion. Front Immunol 7:442. https://doi.org/10.3389/fimmu.2016.00442.
6. Chaconas G, Castellanos M, Verhey TB. 2020. Changing of the guard: how the Lyme disease spirochete subverts the host immune response. J Biol Chem 295:301–313. https://doi.org/10.1074/jbc.REV119.008583.
7. Rana VS, Kitsou C, Dumler JS, Pal U. 2022. Immune evasion strategies of major tick-transmitted bacterial pathogens. Trends Microbiol 31:62–75. https://doi.org/10.1016/j.tim.2022.08.002.
8. Skare JT, Garcia BL. 2020. Complement evasion by Lyme disease spirochetes. Trends Microbiol 28:889–899. https://doi.org/10.1016/j.tim.2020.05.004.
9. Kugeler KJ, Schwartz AM, Delorey MJ, Mead PS, Hinckley AF. 2021. Estimating the frequency of Lyme disease diagnoses, United States, 2010–2018. Emerg Infect Dis 27:616–619. https://doi.org/10.3201/eid2702.202731.
10. Dattwyler RJ, Gomes-Solecki M. 2022. The year that shaped the outcome of the OspA vaccine for human Lyme disease. NPJ Vaccines 7:10. https://doi.org/10.1038/s41541-022-00429-5.
11. Gomes-Solecki M, Arnaboldi PM, Backenson PB, Benach JL, Cooper CL, Dattwyler RJ, Diuk-Wasser M, Fikrig E, Hovius JW, Laegreid W, Lundberg U, Marconi RT, Marques AR, Molloy P, Narasimhan S, Pal U, Pedra JHF, Plotkin S, Rock DL, Rosa P, Telford SR, Tsao J, Yang XF, Schutzer SE. 2020. Protective immunity and new vaccines for Lyme disease. Clin Infect Dis 70:1768–1773. https://doi.org/10.1093/cid/ciz872.
12. Wormser GP. 2022. A brief history of OspA vaccines including their impact on diagnostic testing for Lyme disease. Diagn Microbiol Infect Dis 102:115572. https://doi.org/10.1016/j.diagmicrobio.2021.115572.
13. O'Bier NS, Hatke AL, Camire AC, Marconi RT. 2021. Human and veterinary vaccines for Lyme disease. Curr Issues Mol Biol 42:191–222. https://doi.org/10.21775/cimb.042.191.
14. de Silva AM, Telford SR III, Brunet LR, Barthold SW, Fikrig E. 1996. Borrelia burgdorferi OspA is an arthropod-specific transmission-blocking Lyme disease vaccine. J Exp Med 183:271–275. https://doi.org/10.1084/jem.183.1.271.
15. Fikrig E, Barthold SW, Kantor FS, Flavell RA. 1990. Protection of mice against the Lyme disease agent by immunizing with recombinant OspA. Science 250:553–556. https://doi.org/10.1126/science.2237407.
16. Fikrig E, Telford SR III, Barthold SW, Kantor FS, Spielman A, Flavell RA. 1992. Elimination of Borrelia burgdorferi from vector ticks feeding on OspA-immunized mice. Proc Natl Acad Sci U S A 89:5418–5421. https://doi.org/10.1073/pnas.89.12.5418.
17. Steere AC, Sikand VK, Meurice F, Parenti DL, Fikrig E, Schoen RT, Nowakowski J, Schmid CH, Laukamp S, Buscarino C, Krause DS, Lyme Disease Vaccine Study Group. 1998. Vaccination against Lyme disease with recombinant Borrelia burgdorferi outer-surface lipoprotein A with adjuvant. N Engl J Med 339:209–215. https://doi.org/10.1056/NEJM199807233390401.
18. Nayak A, Schuler W, Seidel S, Gomez I, Meinke A, Comstedt P, Lundberg U. 2020. Broadly protective multivalent OspA vaccine against Lyme borreliosis, developed based on surface shaping of the C-terminal fragment. Infect Immun 88:e00917-19. https://doi.org/10.1128/IAI.00917-19.
19. Wressnigg N, Pöllabauer EM, Aichinger G, Portsmouth D, Löw-Baselli A, Fritsch S, Livey I, Crowe BA, Schwendinger M, Brühl P, Pilz A, Dvorak T, Singer J, Firth C, Luft B, Schmitt B, Zeitlinger M, Müller M, Kollaritsch H, Paulke-Korinek M, Esen M, Kremsner PG, Ehrlich HJ, Barrett PN. 2013. Safety and immunogenicity of a novel multivalent OspA vaccine against Lyme borreliosis in healthy adults: a double-blind, randomised, dose-escalation phase 1/2 trial. Lancet Infect Dis 13:680–689. https://doi.org/10.1016/S1473-3099(13)70110-5.
20. Caimano MJ, Eggers CH, Gonzalez CA, Radolf JD. 2005. Alternate sigma factor RpoS is required for the in vivo-specific repression of Borrelia burgdorferi plasmid lp54-borne ospA and lp6.6 genes. J Bacteriol 187:7845–7852. https://doi.org/10.1128/JB.187.22.7845-7852.2005.
21. Srivastava SY, de Silva AM. 2008. Reciprocal expression of ospA and ospC in single cells of Borrelia burgdorferi. J Bacteriol 190:3429–3433. https://doi.org/10.1128/JB.00085-08.
22. Schwan TG, Piesman J, Golde WT, Dolan MC, Rosa PA. 1995. Induction of an outer surface protein on Borrelia burgdorferi during tick feeding. Proc Natl Acad Sci U S A 92:2909–2913. https://doi.org/10.1073/pnas.92.7.2909.
23. Eicken C, Sharma V, Klabunde T, Owens RT, Pikas DS, Hook M, Sacchettini JC. 2001. Crystal structure of Lyme disease antigen outer surface protein C from Borrelia burgdorferi. J Biol Chem 276:10010–10015. https://doi.org/10.1074/jbc.M010062200.
24. Kumaran D, Eswaramoorthy S, Luft BJ, Koide S, Dunn JJ, Lawson CL, Swaminathan S. 2001. Crystal structure of outer surface protein C (OspC) from the Lyme disease spirochete, Borrelia burgdorferi. EMBO J 20:971–978. https://doi.org/10.1093/emboj/20.5.971.
25. Zückert WR, Kerentseva TA, Lawson CL, Barbour AG. 2001. Structural conservation of neurotropism-associated VspA within the variable Borrelia Vsp-OspC lipoprotein family. J Biol Chem 276:457–463. https://doi.org/10.1074/jbc.M008449200.
26. Ohnishi J, Piesman J, de Silva AM. 2001. Antigenic and genetic heterogeneity of Borrelia burgdorferi populations transmitted by ticks. Proc Natl Acad Sci U S A 98:670–675. https://doi.org/10.1073/pnas.98.2.670.
27. Caimano MJ, Groshong AM, Belperron A, Mao J, Hawley KL, Luthra A, Graham DE, Earnhart CG, Marconi RT, Bockenstedt LK, Blevins JS, Radolf JD. 2019. The RpoS gatekeeper in Borrelia burgdorferi: an invariant regulatory scheme that promotes spirochete persistence in reservoir hosts

and niche diversity. Front Microbiol 10:1923. https://doi.org/10.3389/fmicb.2019.01923.
28. De Silva AM, Fikrig E. 1995. Growth and migration of Borrelia burgdorferi in Ixodes ticks during blood feeding. Am J Trop Med Hyg 53:397–404. https://doi.org/10.4269/ajtmh.1995.53.397.
29. Pal U, Yang X, Chen M, Bockenstedt LK, Anderson JF, Flavell RA, Norgard MV, Fikrig E. 2004. OspC facilitates Borrelia burgdorferi invasion of Ixodes scapularis salivary glands. J Clin Invest 113:220–230. https://doi.org/10.1172/JCI200419894.
30. Gilmore RD, Jr, Kappel KJ, Dolan MC, Burkot TR, Johnson BJ. 1996. Outer surface protein C (OspC), but not P39, is a protective immunogen against a tick-transmitted Borrelia burgdorferi challenge: evidence for a conformational protective epitope in OspC. Infect Immun 64:2234–2239. https://doi.org/10.1128/iai.64.6.2234-2239.1996.
31. Mbow ML, Gilmore RD Jr, Titus RG. 1999. An OspC-specific monoclonal antibody passively protects mice from tick-transmitted infection by Borrelia burgdorferi B31. Infect Immun 67:5470–5472. https://doi.org/10.1128/IAI.67.10.5470-5472.1999.
32. Bhatia B, Hillman C, Carracoi V, Cheff BN, Tilly K, Rosa PA. 2018. Infection history of the blood-meal host dictates pathogenic potential of the Lyme disease spirochete within the feeding tick vector. PLoS Pathog 14:e1006959. https://doi.org/10.1371/journal.ppat.1006959.
33. Bockenstedt LK, Hodzic E, Feng S, Bourrel KW, de Silva A, Montgomery RR, Fikrig E, Radolf JD, Barthold SW. 1997. Borrelia burgdorferi strain-specific Osp C-mediated immunity in mice. Infect Immun 65:4661–4667. https://doi.org/10.1128/iai.65.11.4661-4667.1997.
34. Preac-Mursic V, Wilske B, Jauris S, Will G, Reinhardt S, Lehnert G, Patsouris E, Mehraein P, Soutschek E, Klockmann U. 1992. Active immunization with pC protein of Borrelia burgdorferi protects gerbils against B. burgdorferi infection. Infection 20:342–349. https://doi.org/10.1007/BF01710681.
35. Probert WS, LeFebvre RB. 1994. Protection of C3H/HeN mice from challenge with Borrelia burgdorferi through active immunization with OspA, OspB, or OspC, but not with OspD or the 83-kilodalton antigen. Infect Immun 62:1920–1926. https://doi.org/10.1128/iai.62.5.1920-1926.1994.
36. Zhong W, Stehle T, Museteanu C, Siebers A, Gern L, Kramer M, Wallich R, Simon MM. 1997. Therapeutic passive vaccination against chronic Lyme disease in mice. Proc Natl Acad Sci U S A 94:12533–12538. https://doi.org/10.1073/pnas.94.23.12533.
37. Edmondson DG, Prabhakaran S, Norris SJ, Ullmann AJ, Piesman J, Dolan M, Probst C, Radzimski C, Stöcker W, Komorowski L. 2017. Enhanced protective immunogenicity of homodimeric Borrelia burgdorferi outer surface protein C. Clin Vaccine Immunol 24:e00306-16. https://doi.org/10.1128/CVI.00306-16.
38. Rousselle JC, Callister SM, Schell RF, Lovrich SD, Jobe DA, Marks JA, Wieneke CA. 1998. Borreliacidal antibody production against outer surface protein C of Borrelia burgdorferi. J Infect Dis 178:733–741. https://doi.org/10.1086/515382.
39. Kraiczy P, Hunfeld KP, Peters S, Wurzner R, Acker G, Wilske B, Brade V. 2000. Borreliacidal activity of early Lyme disease sera against complement-resistant Borrelia afzelii FEM1 wild-type and an OspC-lacking FEM1 variant. J Med Microbiol 49:917–928. https://doi.org/10.1099/0022-1317-49-10-917.
40. Bunikis J, Garpmo U, Tsao J, Berglund J, Fish D, Barbour AG. 2004. Sequence typing reveals extensive strain diversity of the Lyme borreliosis agents Borrelia burgdorferi in North America and Borrelia afzelii in Europe. Microbiology (Reading) 150:1741–1755. https://doi.org/10.1099/mic.0.26944-0.
41. Baum E, Randall AZ, Zeller M, Barbour AG. 2013. Inferring epitopes of a polymorphic antigen amidst broadly cross-reactive antibodies using protein microarrays: a study of OspC proteins of Borrelia burgdorferi. PLoS One 8:e67445. https://doi.org/10.1371/journal.pone.0067445.
42. Earnhart CG, Buckles EL, Dumler JS, Marconi RT. 2005. Demonstration of OspC type diversity in invasive human Lyme disease isolates and identification of previously uncharacterized epitopes that define the specificity of the OspC murine antibody response. Infect Immun 73:7869–7877. https://doi.org/10.1128/IAI.73.12.7869-7877.2005.
43. Hanincova K, Mukherjee P, Ogden NH, Margos G, Wormser GP, Reed KD, Meece JK, Vandermause MF, Schwartz I. 2013. Multilocus sequence typing of Borrelia burgdorferi suggests existence of lineages with differential pathogenic properties in humans. PLoS One 8:e73066. https://doi.org/10.1371/journal.pone.0073066.
44. Seinost G, Dykhuizen DE, Dattwyler RJ, Golde WT, Dunn JJ, Wang IN, Wormser GP, Schriefer ME, Luft BJ. 1999. Four clones of Borrelia burgdorferi sensu stricto cause invasive infection in humans. Infect Immun 67:3518–3524. https://doi.org/10.1128/IAI.67.7.3518-3524.1999.
45. Wang IN, Dykhuizen DE, Qiu W, Dunn JJ, Bosler EM, Luft BJ. 1999. Genetic diversity of ospC in a local population of Borrelia burgdorferi sensu stricto. Genetics 151:15–30. https://doi.org/10.1093/genetics/151.1.15.
46. Barbour AG, Travinsky B. 2010. Evolution and distribution of the ospC Gene, a transferable serotype determinant of Borrelia burgdorferi. mBio 1:e00153-10. https://doi.org/10.1128/mBio.00153-10.
47. Di L, Akther S, Bezrucenkovas E, Ivanova L, Sulkow B, Wu B, Mneimneh S, Gomes-Solecki M, Qiu WG. 2022. Maximum antigen diversification in a Lyme bacterial population and evolutionary strategies to overcome pathogen diversity. ISME J 16:447–464. https://doi.org/10.1038/s41396-021-01089-4.
48. Khatchikian CE, Nadelman RB, Nowakowski J, Schwartz I, Wormser GP, Brisson D. 2014. Evidence for strain-specific immunity in patients treated for early Lyme disease. Infect Immun 82:1408–1413. https://doi.org/10.1128/IAI.01451-13.
49. Nadelman RB, Hanincova K, Mukherjee P, Liveris D, Nowakowski J, McKenna D, Brisson D, Cooper D, Bittker S, Madison G, Holmgren D, Schwartz I, Wormser GP. 2012. Differentiation of reinfection from relapse in recurrent Lyme disease. N Engl J Med 367:1883–1890. https://doi.org/10.1056/NEJMoa1114362.
50. Earnhart CG, Marconi RT. 2007. OspC phylogenetic analyses support the feasibility of a broadly protective polyvalent chimeric Lyme disease vaccine. Clin Vaccine Immunol 14:628–634. https://doi.org/10.1128/CVI.00409-06.
51. Earnhart CG, Leblanc DV, Alix KE, Desrosiers DC, Radolf JD, Marconi RT. 2010. Identification of residues within ligand-binding domain 1 (LBD1) of the Borrelia burgdorferi OspC protein required for function in the mammalian environment. Mol Microbiol 76:393–408. https://doi.org/10.1111/j.1365-2958.2010.07103.x.
52. Izac JR, Camire AC, Earnhart CG, Embers ME, Funk RA, Breitschwerdt EB, Marconi RT. 2019. Analysis of the antigenic determinants of the OspC protein of the Lyme disease spirochetes: Evidence that the C10 motif is not immunodominant or required to elicit bactericidal antibody responses. Vaccine 37:2401–2407. https://doi.org/10.1016/j.vaccine.2019.02.007.
53. Izac JR, O'Bier NS, Oliver LD Jr, Camire AC, Earnhart CG, LeBlanc Rhodes DV, Young BF, Parnham SR, Davies C, Marconi RT. 2020. Development and optimization of OspC chimeritope vaccinogens for Lyme disease. Vaccine 38:1915–1924. https://doi.org/10.1016/j.vaccine.2020.01.027.
54. Norek A, Janda L. 2017. Epitope mapping of Borrelia burgdorferi OspC protein in homodimeric fold. Protein Sci 26:796–806. https://doi.org/10.1002/pro.3125.
55. Wilske B, Luft B, Schubach WH, Zumstein G, Jauris S, Preac-Mursic V, Kramer MD. 1992. Molecular analysis of the outer surface protein A (OspA) of Borrelia burgdorferi for conserved and variable antibody binding domains. Med Microbiol Immunol 181:191–207. https://doi.org/10.1007/BF00215765.
56. Marconi RT, Garcia-Tapia D, Hoevers J, Honsberger N, King VL, Ritter D, Schwahn DJ, Swearingin L, Weber A, Winkler MTC, Millership J. 2020. VANGUARD(R)crLyme: A next generation Lyme disease vaccine that prevents B. burgdorferi infection in dogs. Vaccine X 6:100079. https://doi.org/10.1016/j.jvacx.2020.100079.
57. Earnhart CG, Marconi RT. 2007. Construction and analysis of variants of a polyvalent Lyme disease vaccine: approaches for improving the immune response to chimeric vaccinogens. Vaccine 25:3419–3427. https://doi.org/10.1016/j.vaccine.2006.12.051.
58. Izac JR, Marconi RT. 2019. Diversity of the Lyme disease spirochetes and its influence on immune responses to infection and vaccination. Vet Clin North Am Small Anim Pract 49:671–686. https://doi.org/10.1016/j.cvsm.2019.02.007.
59. Crowe JE Jr. 2017. Principles of broad and potent antiviral human antibodies: insights for vaccine design. Cell Host Microbe 22:193–206. https://doi.org/10.1016/j.chom.2017.07.013.
60. Rappuoli R, Bottomley MJ, D'Oro U, Finco O, De Gregorio E. 2016. Reverse vaccinology 2.0: Human immunology instructs vaccine antigen design. J Exp Med 213:469–481. https://doi.org/10.1084/jem.20151960.
61. Walker LM, Burton DR. 2010. Rational antibody-based HIV-1 vaccine design: current approaches and future directions. Curr Opin Immunol 22:358–366. https://doi.org/10.1016/j.coi.2010.02.012.
62. Comstedt P, Hanner M, Schuler W, Meinke A, Lundberg U. 2014. Design and development of a novel vaccine for protection against Lyme borreliosis. PLoS One 9:e113294. https://doi.org/10.1371/journal.pone.0113294.
63. Ding W, Huang X, Yang X, Dunn JJ, Luft BJ, Koide S, Lawson CL. 2000. Structural identification of a key protective B-cell epitope in Lyme

disease antigen OspA. J Mol Biol 302:1153–1164. https://doi.org/10.1006/jmbi.2000.4119.
64. Schiller ZA, Rudolph MJ, Toomey JR, Ejemel M, LaRochelle A, Davis SA, Lambert HS, Kern A, Tardo AC, Souders CA, Peterson E, Cannon RD, Ganesa C, Fazio F, Mantis NJ, Cavacini LA, Sullivan-Bolyai J, Hu LT, Embers ME, Klempner MS, Wang Y. 2021. Blocking Borrelia burgdorferi transmission from infected ticks to nonhuman primates with a human monoclonal antibody. J Clin Invest 131:e144843. https://doi.org/10.1172/JCI144843.
65. Mbow ML, Gilmore RD Jr, Stevenson B, Golde WT, Piesman J, Johnson BJ. 2002. Borrelia burgdorferi-specific monoclonal antibodies derived from mice primed with Lyme disease spirochete-infected Ixodes scapularis ticks. Hybrid Hybridomics 21:179–182. https://doi.org/10.1089/153685902760173890.
66. Gilmore RD Jr, Piesman J. 2000. Inhibition of Borrelia burgdorferi migration from the midgut to the salivary glands following feeding by ticks on OspC-immunized mice. Infect Immun 68:411–414. https://doi.org/10.1128/IAI.68.1.411-414.2000.
67. Liang FT, Jacobs MB, Bowers LC, Philipp MT. 2002. An immune evasion mechanism for spirochetal persistence in Lyme borreliosis. J Exp Med 195:415–422. https://doi.org/10.1084/jem.20011870.
68. Gilmore RD Jr, Mbow ML. 1999. Conformational nature of the Borrelia burgdorferi B31 outer surface protein C protective epitope. Infect Immun 67:5463–5469. https://doi.org/10.1128/IAI.67.10.5463-5469.1999.
69. Angalakurthi SK, Vance DJ, Rong Y, Nguyen CMT, Rudolph MJ, Volkin D, Middaugh CR, Weis DD, Mantis NJ. 2018. A collection of single-domain antibodies that crowd ricin toxin's active site. Antibodies (Basel) 7:45. https://doi.org/10.3390/antib7040045.
70. Brier S, Rasetti-Escargueil C, Wijkhuisen A, Simon S, Marechal M, Lemichez E, Popoff MR. 2021. Characterization of a highly neutralizing single monoclonal antibody to botulinum neurotoxin type A. FASEB J 35:e21540. https://doi.org/10.1096/fj.202002492R.
71. Chen G, Karauzum H, Long H, Carranza D, Holtsberg FW, Howell KA, Abaandou L, Zhang B, Jarvik N, Ye W, Liao GC, Gross ML, Leung DW, Amarasinghe GK, Aman MJ, Sidhu SS. 2019. Potent neutralization of Staphylococcal enterotoxin B in vivo by antibodies that block binding to the T-cell receptor. J Mol Biol 431:4354–4367. https://doi.org/10.1016/j.jmb.2019.03.017.
72. Hodge EA, Naika GS, Kephart SM, Nguyen A, Zhu R, Benhaim MA, Guo W, Moore JP, Hu SL, Sanders RW, Lee KK. 2022. Structural dynamics reveal isolate-specific differences at neutralization epitopes on HIV Env. iScience 25:104449. https://doi.org/10.1016/j.isci.2022.104449.
73. Seow J, Khan H, Rosa A, Calvaresi V, Graham C, Pickering S, Pye VE, Cronin NB, Huettner I, Malim MH, Politis A, Cherepanov P, Doores KJ. 2022. A neutralizing epitope on the SD1 domain of SARS-CoV-2 spike targeted following infection and vaccination. Cell Rep 40:111276. https://doi.org/10.1016/j.celrep.2022.111276.
74. Grauslund LR, Calvaresi V, Pansegrau W, Norais N, Rand KD. 2021. Epitope and paratope mapping by HDX-MS combined with SPR elucidates the difference in bactericidal activity of two anti-NadA monoclonal antibodies. J Am Soc Mass Spectrom 32:1575–1582. https://doi.org/10.1021/jasms.0c00431.
75. Malito E, Faleri A, Lo Surdo P, Veggi D, Maruggi G, Grassi E, Cartocci E, Bertoldi I, Genovese A, Santini L, Romagnoli G, Borgogni E, Brier S, Lo Passo C, Domina M, Castellino F, Felici F, van der Veen S, Johnson S, Lea SM, Tang CM, Pizza M, Savino S, Norais N, Rappuoli R, Bottomley MJ, Masignani V. 2013. Defining a protective epitope on factor H binding protein, a key meningococcal virulence factor and vaccine antigen. Proc Natl Acad Sci U S A 110:3304–3309. https://doi.org/10.1073/pnas.1222845110.
76. Vinciauskaite V, Masson GR. 2022. Fundamentals of HDX-MS. Essays Biochem https://doi.org/10.1042/EBC20220111.
77. Haque HME, Ejemel M, Vance DJ, Willsey G, Rudolph MJ, Cavacini LA, Wang Y, Mantis NJ, Weis DD. 2022. Human B cell epitope map of the Lyme disease vaccine antigen, OspA. ACS Infect Dis 18:2515–2528. https://doi.org/10.1021/acsinfecdis.2c00346.
78. Liang FT, Yan J, Mbow ML, Sviat SL, Gilmore RD, Mamula M, Fikrig E. 2004. Borrelia burgdorferi changes its surface antigenic expression in response to host immune responses. Infect Immun 72:5759–5767. https://doi.org/10.1128/IAI.72.10.5759-5767.2004.
79. Xu Q, Seemanapalli SV, McShan K, Liang FT. 2006. Constitutive expression of outer surface protein C diminishes the ability of Borrelia burgdorferi to evade specific humoral immunity. Infect Immun 74:5177–5184. https://doi.org/10.1128/IAI.00713-06.
80. Rudolph MJ, Poon AY, Kavaliauskiene S, Myrann AG, Reynolds-Peterson C, Davis SA, Sandvig K, Vance DJ, Mantis NJ. 2021. Structural analysis of toxin-neutralizing, single-domain antibodies that bridge ricin's A-B subunit interface. J Mol Biol 433:167086. https://doi.org/10.1016/j.jmb.2021.167086.
81. Milligan JC, Davis CW, Yu X, Ilinykh PA, Huang K, Halfmann PJ, Cross RW, Borisevich V, Agans KN, Geisbert JB, Chennareddy C, Goff AJ, Piper AE, Hui S, Shaffer KCL, Buck T, Heinrich ML, Branco LM, Crozier I, Holbrook MR, Kuhn JH, Kawaoka Y, Glass PJ, Bukreyev A, Geisbert TW, Worwa G, Ahmed R, Saphire EO. 2022. Asymmetric and non-stoichiometric glycoprotein recognition by two distinct antibodies results in broad protection against ebolaviruses. Cell 185:995–1007.e18. https://doi.org/10.1016/j.cell.2022.02.023.
82. Tortorici MA, Beltramello M, Lempp FA, Pinto D, Dang HV, Rosen LE, McCallum M, Bowen J, Minola A, Jaconi S, Zatta F, De Marco A, Guarino B, Bianchi S, Lauron EJ, Tucker H, Zhou J, Peter A, Havenar-Daughton C, Wojcechowskyj JA, Case JB, Chen RE, Kaiser H, Montiel-Ruiz M, Meury M, Czudnochowski N, Spreafico R, Dillen J, Ng C, Sprugasci N, Culap K, Benigni F, Abdelnabi R, Foo SC, Schmid MA, Cameroni E, Riva A, Gabrieli A, Galli M, Pizzuto MS, Neyts J, Diamond MS, Virgin HW, Snell G, Corti D, Fink K, Veesler D. 2020. Ultrapotent human antibodies protect against SARS-CoV-2 challenge via multiple mechanisms. Science 370:950–957. https://doi.org/10.1126/science.abe3354.
83. Wu NC, Wilson IA. 2020. Structural biology of influenza hemagglutinin: an amaranthine adventure. Viruses 12:1053. https://doi.org/10.3390/v12091053.
84. Blum ML, Down JA, Gurnett AM, Carrington M, Turner MJ, Wiley DC. 1993. A structural motif in the variant surface glycoproteins of Trypanosoma brucei. Nature 362:603–609. https://doi.org/10.1038/362603a0.
85. Eicken C, Sharma V, Klabunde T, Lawrenz MB, Hardham JM, Norris SJ, Sacchettini JC. 2002. Crystal structure of Lyme disease variable surface antigen VlsE of Borrelia burgdorferi. J Biol Chem 277:21691–21696. https://doi.org/10.1074/jbc.M201547200.
86. Hempelmann A, Hartleb L, van Straaten M, Hashemi H, Zeelen JP, Bongers K, Papavasiliou FN, Engstler M, Stebbins CE, Jones NG. 2021. Nanobody-mediated macromolecular crowding induces membrane fission and remodeling in the African trypanosome. Cell Rep 37:109923. https://doi.org/10.1016/j.celrep.2021.109923.
87. Toledo A, Crowley JT, Coleman JL, LaRocca TJ, Chiantia S, London E, Benach JL. 2014. Selective association of outer surface lipoproteins with the lipid rafts of Borrelia burgdorferi. mBio 5:e00899-14. https://doi.org/10.1128/mBio.00899-14.
88. Wang Y, Kern A, Boatright NK, Schiller ZA, Sadowski A, Ejemel M, Souders CA, Reimann KA, Hu L, Thomas WD Jr, Klempner MS. 2016. Pre-exposure prophylaxis with OspA-specific human monoclonal antibodies protects mice against tick transmission of Lyme disease spirochetes. J Infect Dis 214:205–211. https://doi.org/10.1093/infdis/jiw151.
89. Sadziene A, Wilske B, Ferdows MS, Barbour AG. 1993. The cryptic ospC gene of Borrelia burgdorferi B31 is located on a circular plasmid. Infect Immun 61:2192–2195. https://doi.org/10.1128/iai.61.5.2192-2195.1993.
90. Rong Y, Torres-Velez FJ, Ehrbar D, Doering J, Song R, Mantis NJ. 2020. An intranasally administered monoclonal antibody cocktail abrogates ricin toxin-induced pulmonary tissue damage and inflammation. Hum Vaccin Immunother 16:793–807. https://doi.org/10.1080/21645515.2019.1664243.
91. Wang L, Pan H, Smith DL. 2002. Hydrogen exchange-mass spectrometry: optimization of digestion conditions. Mol Cell Proteomics 1:132–138. https://doi.org/10.1074/mcp.M100009-MCP200.
92. Otwinowski Z, Minor W. 1997. Processing of x-ray diffraction data collected in oscillation mode. Methods Enzymol 276:307–326. https://doi.org/10.1016/S0076-6879(97)76066-X.
93. Winn MD, Ballard CC, Cowtan KD, Dodson EJ, Emsley P, Evans PR, Keegan RM, Krissinel EB, Leslie AG, McCoy A, McNicholas SJ, Murshudov GN, Pannu NS, Potterton EA, Powell HR, Read RJ, Vagin A, Wilson KS. 2011. Overview of the CCP4 suite and current developments. Acta Crystallogr D Biol Crystallogr 67:235–242. https://doi.org/10.1107/S0907444910045749.
94. Emsley P, Lohkamp B, Scott WG, Cowtan K. 2010. Features and development of Coot. Acta Crystallogr D Biol Crystallogr 66:486–501. https://doi.org/10.1107/S0907444910007493.
95. Adams PD, Afonine PV, Bunkoczi G, Chen VB, Davis IW, Echols N, Headd JJ, Hung LW, Kapral GJ, Grosse-Kunstleve RW, McCoy AJ, Moriarty NW, Oeffner R, Read RJ, Richardson DC, Richardson JS, Terwilliger TC, Zwart PH. 2010. PHENIX: a comprehensive Python-based system for macromolecular structure solution. Acta Crystallogr D Biol Crystallogr 66:213–221. https://doi.org/10.1107/S0907444909052925.
96. Pulzova L, Flachbartova Z, Bencurova E, Potocnakova L, Comor L, Schreterova E, Bhide M. 2016. Identification of B-cell epitopes of Borrelia burgdorferi outer surface protein C by screening a phage-displayed gene fragment library. Microbiol Immunol 60:669–677. https://doi.org/10.1111/1348-0421.12438.

97. Yu Z, Carter JM, Sigal LH, Stein S. 1996. Multi-well ELISA based on independent peptide antigens for antibody capture. Application to Lyme disease serodiagnosis. J Immunol Methods 198:25–33. https://doi.org/10.1016/0022-1759(96)00140-8.
98. Buckles EL, Earnhart CG, Marconi RT. 2006. Analysis of antibody response in humans to the type A OspC loop 5 domain and assessment of the potential utility of the loop 5 epitope in Lyme disease vaccine development. Clin Vaccine Immunol 13:1162–1165. https://doi.org/10.1128/CVI.00099-06.
99. Arnaboldi PM, Seedarnee R, Sambir M, Callister SM, Imparato JA, Dattwyler RJ. 2013. Outer surface protein C peptide derived from Borrelia burgdorferi sensu stricto as a target for serodiagnosis of early Lyme disease. Clin Vaccine Immunol 20:474–481. https://doi.org/10.1128/CVI.00608-12.
100. Mathiesen MJ, Holm A, Christiansen M, Blom J, Hansen K, Ostergaard S, Theisen M. 1998. The dominant epitope of Borrelia garinii outer surface protein C recognized by sera from patients with neuroborreliosis has a surface-exposed conserved structural motif. Infect Immun 66:4073–4079. https://doi.org/10.1128/IAI.66.9.4073-4079.1998.